

# The Transient Atmospheric Circulation Response to North Atlantic SST and Sea Ice Anomalies

CLARA DESER AND ROBERT A. TOMAS

*National Center for Atmospheric Research, Boulder, Colorado*

SHILING PENG

*NOAA/Earth System Research Laboratory, Boulder, Colorado*

(Manuscript received 28 July 2006, in final form 12 February 2007)

## ABSTRACT

The objective of this study is to investigate the transient evolution of the wintertime atmospheric circulation response to imposed patterns of SST and sea ice extent anomalies in the North Atlantic sector using a large ensemble of experiments with the NCAR Community Climate Model version 3 (CCM3). The initial adjustment of the atmospheric circulation is characterized by an out-of-phase relationship between geopotential height anomalies in the lower and upper troposphere localized to the vicinity of the forcing. This initial baroclinic response reaches a maximum amplitude in  $\sim 5$ – $10$  days, and persists for 2–3 weeks. Diagnostic results with a linear primitive equation model indicate that this initial response is forced by diabatic heating anomalies in the lower troposphere associated with surface heat flux anomalies generated by the imposed thermal forcing. Following the initial baroclinic stage of adjustment, the response becomes progressively more barotropic and increases in both spatial extent and magnitude. The equilibrium stage of adjustment is reached in 2–2.5 months, and is characterized by an equivalent barotropic structure that resembles the hemispheric North Atlantic Oscillation–Northern Annular Mode (NAO–NAM) pattern, the model’s leading internal mode of circulation variability over the Northern Hemisphere. The maximum amplitude of the equilibrium response is approximately 2–3 times larger than that of the initial response. The equilibrium response is primarily maintained by nonlinear transient eddy fluxes of vorticity (and, to a lesser extent, heat), with diabatic heating making a limited contribution in the vicinity of the forcing.

## 1. Introduction

Considerable progress has been made over the past decade in understanding the mechanisms generating the equilibrium atmospheric circulation response to extratropical SST anomalies (Robinson 2000; Kushnir et al. 2002; Peng et al. 2003). It is now clear that the equilibrium response depends upon the nature and strength of transient eddy feedbacks, particularly eddy vorticity fluxes, resulting from interactions between the heating-forced anomalous flow and the storm tracks (Kushnir and Lau 1992; Ting and Peng 1995; Peng and Whitaker 1999; Peng et al. 2003). These transient eddy feedbacks may substantially modify the direct baroclinic response

to anomalous diabatic heating (Hoskins and Karoly 1981; Hendon and Hartmann 1982) into an equivalent barotropic response that extends well beyond the region of forcing (Peng et al. 2003; Magnúsdóttir et al. 2004). Thus, different atmospheric models may produce different responses to the same SST anomaly depending on their simulation of the location and intensity of the climatological mean storm tracks (Peng and Whitaker 1999; Walter et al. 2001; Hall et al. 2001). Another important and related factor influencing the atmospheric response to extratropical SST anomalies is the structure of the model’s intrinsic variability, which is known to be mainly eddy driven (Branstator 1992; Ting and Lau 1993). Depending on the location of the SST forcing, the response may project onto the dominant modes of internal atmospheric variability thereby changing their frequency of occurrence (Peng and Robinson 2001; Hall et al. 2001; Peng et al. 2003; Magnúsdóttir et al. 2004; Deser et al. 2004; Cassou et al. 2007).

---

*Corresponding author address:* Dr. Clara Deser, Climate and Global Dynamics Division, NCAR, P.O. Box 3000, Boulder, CO 80307-3000.

E-mail: cdeser@ucar.edu

DOI: 10.1175/JCLI4278.1

Thus, models with different structures of intrinsic variability may produce different hemispheric-wide responses to the same SST anomaly.

All of the studies cited above are based upon diagnosis of the equilibrium atmospheric response to extratropical SST anomalies. An alternative approach is to examine the transient adjustment of the atmospheric circulation to imposed thermal forcing. Two recent modeling studies, Li and Conil (2003) and Ferreira and Frankignoul (2005), have investigated aspects of this adjustment process to North Atlantic SST anomalies. Li and Conil (2003) examined the initial (days 1–8) transient evolution of the atmospheric response over the North Atlantic and Europe to an observed tripole pattern of SST anomalies in the North Atlantic based on a 240-member ensemble of perpetual January integrations of the Laboratoire de Météorologie Dynamique Zoom (LMDZ) general circulation model (GCM), a 19-level model with approximately 60-km horizontal resolution over the North Atlantic (Li 1999). They found that initially (days 1–2) the response is baroclinic and localized to the vicinity of the forcing, while over the next 6 days the response becomes more barotropic and exhibits some downstream development. However, the limited duration of their experiments (8 days) did not allow them to assess how long it takes for the response to come to equilibrium, and their focus on the North Atlantic–European sector did not afford an examination of the full spatial scale of the response.

Ferreira and Frankignoul (2005) examined the atmospheric response to a North Atlantic SST tripole anomaly pattern similar to that in Li and Conil (2003) using a three-level quasigeostrophic model solved at T31 resolution (approximately  $3.75^\circ$  latitude and  $3.75^\circ$  longitude) under perpetual wintertime conditions. They conducted a 400-member ensemble of integrations each 10 months in duration, long enough to reach equilibrium. They found that the initial atmospheric response is forced by diabatic heating anomalies associated with anomalous air–sea heat fluxes and its structure is similar to that predicted by linear theory. This initial circulation response rapidly modifies the transient eddy activity, which in turn transforms the initial baroclinic response into an equivalent barotropic one. This equivalent barotropic response resembles the anomalous atmospheric circulation pattern that created the SST tripole anomaly in the first place (determined from experiments with an interactive ocean mixed layer model), thus acting as a positive feedback. The adjustment time for the establishment of the barotropic response was 3–4 months for the circulation pattern resembling the North Atlantic Oscillation–Northern Annular Mode (NAO–NAM; Hurrell 1995; Thompson

and Wallace 1998), the leading structure of internal wintertime atmospheric variability over the Northern Hemisphere. It remains to be seen whether the adjustment time in a three-level quasigeostrophic model is indicative of that in a more complex atmospheric GCM.

Deser et al. (2004, hereafter D04) and the companion study of Magnúsdóttir et al. (2004, hereafter M04) used an atmospheric GCM to examine the equilibrium circulation response to two types of boundary forcing: sea ice and SST. These boundary forcings were specified to have realistic spatial patterns based on observed trends over the North Atlantic sector during the second half of the twentieth century. Varying the magnitude and sign of the forcing patterns, D04 and M04 found that the responses scaled linearly with amplitude but nonlinearly with polarity. For the cases of SST forcing with reversed polarity (consisting mainly of a positive anomaly in the subpolar gyre) and sea ice forcing with observed polarity (reduced ice extent in the Greenland and Barents Seas and increased ice extent in the Labrador Sea), the wintertime atmospheric circulation responses were found to be very similar, resembling the negative phase of the NAO–NAM, the leading mode of variability in a long control run of the model.

D04 partitioned these responses into a component that projects onto the leading mode of internal variability and a residual from that projection. They found that these two components of the response exhibit distinctive vertical and spatial structures, suggestive of different underlying dynamical mechanisms. In particular, the residual component exhibits a baroclinic vertical structure confined to the vicinity of the forcing, while the internal projection component exhibits an equivalent barotropic vertical structure that is hemispheric in scale. This empirical separation of the response into two distinct components led them to speculate that the residual component is maintained by diabatic heating anomalies associated with the surface boundary forcing and that the internal projection component is maintained primarily by transient eddy flux convergences of heat and vorticity, as suggested in earlier mechanistic studies (e.g., Ting and Peng 1995; Peng and Whitaker 1999; Peng and Robinson 2001).

The objective of this study is to further our understanding of the nature of the transient evolution of the atmospheric circulation response to mid- and high-latitude SST and sea ice forcing using experiments with the National Center for Atmospheric Research (NCAR) Community Climate Model version 3 (CCM3). The SST and sea ice forcing patterns are identical to those in D04 and M04 described above. To enhance the robustness of the results, we conduct a large (240 member) ensemble of simulations for each type of boundary forc-

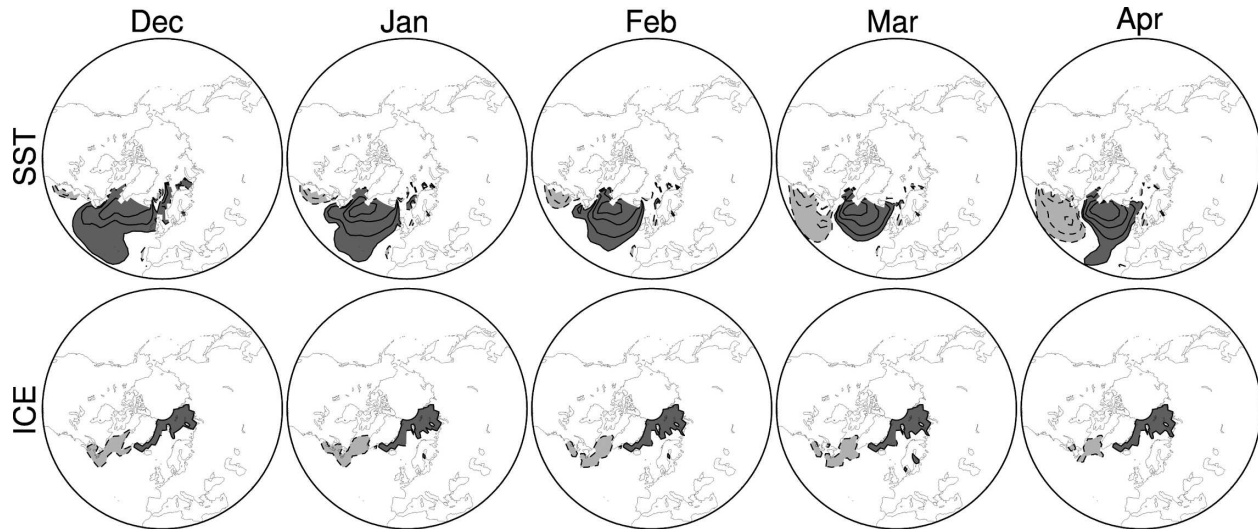


FIG. 1. (top) Monthly SST anomalies used to force CCM3, the SST experiment. Solid contours and dark shading denote positive anomalies; dashed contours and light shading denote negative anomalies. The contour interval is 2 K and only odd numbered contours are shown (e.g.,  $\pm 1$  K, 3 K, ...). (Bottom) Monthly sea ice extent anomalies used to force CCM3, the ICE experiment. Areas enclosed by dark (light) shading denote regions where sea ice has been removed from (added to) the climatological distribution.

ing, as well as comparing the ensemble mean responses to sea ice *versus* SST forcing. We employ a linear atmospheric primitive equation model to diagnose the maintenance of the transient response at different stages of its evolution. Our investigation is guided by the following questions. What are the structures of the initial and equilibrium responses, and what are the processes that maintain them? What is the adjustment time for the establishment of the equilibrium response? Is there a physical basis for the empirical decomposition of the equilibrium response performed in D04?

The paper is structured as follows: section 2 describes the experiments with CCM3 and the linear primitive equation model; section 3 presents the results; and Section 4 provides a discussion and conclusions.

## 2. Model experiments

### a. CCM3

The spatial patterns of the North Atlantic SST and sea ice anomalies used to force CCM3 are identical to those in D04 and are based upon observed trends during the second half of the twentieth century. For the present study, we have selected the amplitude and polarity of the forcing patterns that D04 found gave the strongest and most similar responses (e.g., the negative phase of the NAO–NAM). Specifically, the SST forcing is defined as the observed SST trend computed separately for each month from the Global Sea Ice and Sea Surface Temperature version 2 dataset (GISST2) dataset (Raynor et al. 1996) during 1954–94 over the

North Atlantic north of  $30^{\circ}\text{N}$ , multiplied by a factor of  $-5$  (i.e., the polarity of the observed trend is reversed and its amplitude magnified fivefold). Similarly, the sea ice forcing is defined as the observed monthly trend in sea ice extent over the North Atlantic–Arctic region during 1958–97 from Deser et al. (2000), multiplied by approximately a factor of 2. Note that a grid cell is either ice free or 100% ice covered; there is no fractional ice concentration. Since sea ice is not explicitly represented in the model, only surface properties such as albedo and the surface energy fluxes change when the sea surface is covered by ice. Both the monthly SST and sea ice forcings were linearly interpolated to daily values and applied as anomalies upon the mean seasonal cycle.

Figure 1 shows the monthly SST and sea ice anomaly forcing fields during December–April, the period of the model experiments. The SST forcing field exhibits some evolution over the course of the winter. In December–February, the main anomaly is positive and located in the subpolar gyre, with a maximum amplitude of  $\sim 7$  K in February; a weaker negative anomaly is found off the east coast of North America (maximum amplitude 3 K). In late winter (March–April), the two anomaly centers are approximately equal in amplitude and area extent. The sea ice forcing is nearly constant over the course of the winter, consisting of a reduction in sea ice cover in the Greenland Sea and an extension of the ice edge in the Labrador Sea.

Two sets of anomaly experiments were conducted: one in which CCM3 is forced with the SST anomalies

and the sea ice extent is held fixed at its seasonally varying climatological values, and one in which the model is forced with the sea ice anomalies and the SST field is set to its climatological seasonal cycle. Each set of experiments, hereafter referred to as “SST” and “ICE,” consists of a 240-member ensemble of 5-month integrations starting on 1 December and ending on 30 April. The atmospheric initial conditions are different for each ensemble member and were obtained from long control runs with no anomalous forcing. In addition to the two sets of anomaly experiments, a 240-member control ensemble was conducted with no anomalies applied to either the SST or sea ice fields. The initial conditions for this control ensemble are identical to those used in the anomaly experiments. Thus, one can think of the experiments as consisting of a pair of integrations (one with and one without boundary forcing), with each member of the pair starting from the same initial conditions, but different initial conditions used for each of the 240 pairs.

To obtain the atmospheric response to the prescribed SST or sea ice anomaly forcing, the control experiment was subtracted from its paired anomaly experiment for each day of the integration; the daily ensemble mean response was then defined by averaging the 240 individual member responses. Statistical significance was assessed by means of a two-sided Student’s  $t$  test.

As stated in the introduction, we used the NCAR CCM3 in the standard configuration as detailed in Kiehl et al. (1998) to be consistent with the earlier experiments of D04. CCM3 has a horizontal resolution of approximately  $2.8^\circ$  latitude and  $2.8^\circ$  longitude (T42 spectral truncation) with 18 vertical layers in a hybrid-sigma coordinate system. The reader is referred to Hack et al. (1998) and Hurrell et al. (1998) for assessments of the hydrologic, thermodynamic, and dynamical characteristics of CCM3.

#### *b. Linear baroclinic model*

To understand the mechanisms for the CCM3 atmospheric circulation response to SST or sea ice anomalies, we force a linear baroclinic model (LBM) with the diabatic heating and transient eddy heat and vorticity fluxes from the SST and ICE GCM experiments. The LBM, the same as that used in Peng et al. (2003), is based on the primitive equations configured with T21 horizontal resolution and 10 equally spaced pressure levels from 950 to 50 hPa. The model is linearized about the CCM3 basic state based on the mean of the 240 control integrations. Two periods (1 December–15 January and 15 January–15 April) are used for defining the basic state since the evolution of the basic state over the course of the winter may impact the response to

anomalous forcing; however, sensitivity experiments with the basic state for different periods indicate the change in the LBM results presented here is small (not shown). The LBM includes dissipation in the form of Rayleigh friction in the momentum equations and Newtonian cooling in the thermodynamic equation, as well as biharmonic thermal diffusion. The Rayleigh and Newtonian damping time scales are 1 day at 950 hPa transitioning linearly to 7 days above 700 hPa, identical to those used in Peng et al. We have repeated all of the analyses with a damping time scale of 10 days above 700 hPa (not shown), with the result that the LBM responses are slightly stronger with the reduced damping, as expected; however, given the arbitrary nature of the dissipation formulation, we have chosen not to tune these coefficients. The LBM is integrated for 50 days, having reached a steady solution by  $\sim 15$ – $20$  days (not shown). Note that the LBM is being used in a diagnostic sense to determine the relative contributions of diabatic heating and transient eddy heat and vorticity fluxes to the dynamical maintenance of the response, not in a prognostic sense (e.g., the time scale of the LBM response is irrelevant to our purpose).

The maintenance of the CCM3 response to SST and sea ice forcing is diagnosed by comparing the LBM responses to the anomalous diabatic heating and transient eddy heat and vorticity fluxes from the SST and ICE experiments. Transient eddies are defined by subtracting 11-day running means from the raw daily data (the half-power point of this filter is 14 days). To avoid loss of information at the end points of the integrations, the transients for the first and last week are defined as daily departures from the time means of the first and last week, respectively.

### **3. Results**

#### *a. Geopotential height response*

The first 5 days (2–6 December) of the ensemble mean geopotential height responses at 1000 and 300 hPa are shown in Fig. 2 for the SST and ICE experiments (note that 2 December is the first full day of the integrations). The responses are localized to the vicinity of the boundary forcing, particularly at 1000 hPa, and exhibit a baroclinic structure in the vertical, with an anomalous surface low (high) over positive (negative) surface temperature anomalies, accompanied by an anomalous ridge (trough) aloft. This response amplifies with time, reaching maximum values  $\sim 40$  m at 300 hPa on 6 December. The responses are statistically significant at the 95% confidence level based on a Student’s  $t$  test, as indicated by the shaded regions in Fig. 2.

Figures 3a,b show the full evolution of the weekly

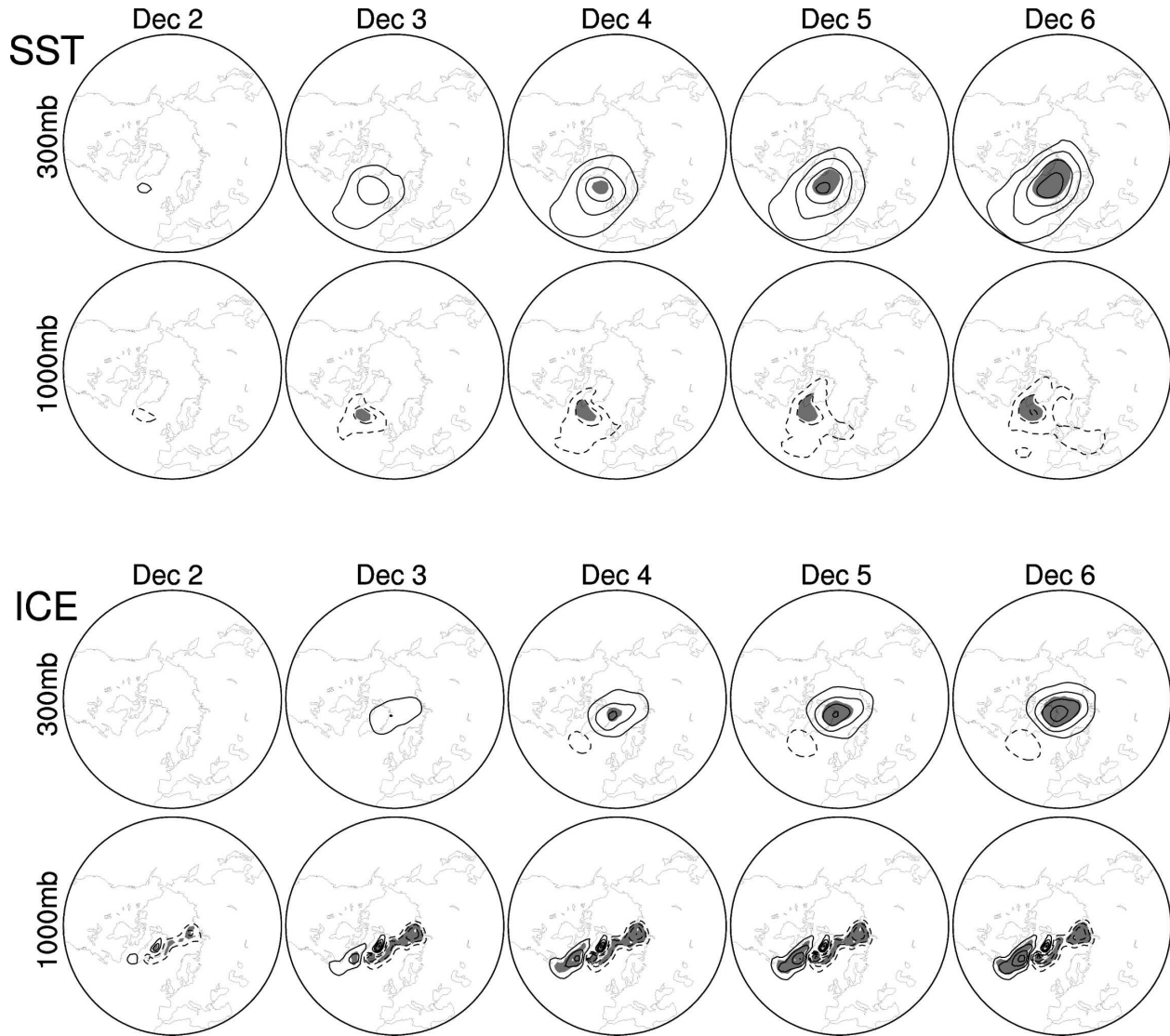


FIG. 2. Ensemble-mean 1000- and 300-hPa geopotential height responses for the first 5 days of the (top) SST and (bottom) ICE experiments. The contour interval is 10 m, with solid (dashed) contours denoting positive (negative) values; the zero contour has been omitted for clarity. Shading denotes values significant at the 95% confidence level based on a two-sided Student's  $t$  test.

averaged ensemble mean geopotential height responses at 1000 and 300 hPa over the course of the winter (December–April) for the SST and ICE experiments, respectively. To fit all the weeks onto a single diagram, every other week is omitted starting in February. The initial localized baroclinic response evolves into a near-hemispheric equivalent barotropic pattern after approximately 6–7 weeks. This hemispheric pattern is maintained for most of the remaining winter, although individual anomaly centers fluctuate in their amplitude and location. The initial localized response pattern may still be seen embedded within the larger-scale response at 1000 hPa, especially in the ICE case. Once the hemispheric equivalent barotropic pattern becomes estab-

lished (early–mid-January), the SST and ICE responses are similar in their gross features especially at 300 hPa, with positive anomalies over high latitudes and negative anomalies in midlatitudes. However, the negative anomaly over the North Atlantic tends to be located farther poleward in the ICE case compared to the SST case, with a concurrent shift in the positive anomaly center to the north. This poleward shift is in keeping with the northward shift of the location of the forcing in the two experiments (cf. Fig. 1). The response over the North Pacific is weaker in the ICE case than the SST case during late January–mid-February.

The vertical structure of the geopotential height response as a function of time is summarized in Fig. 4,

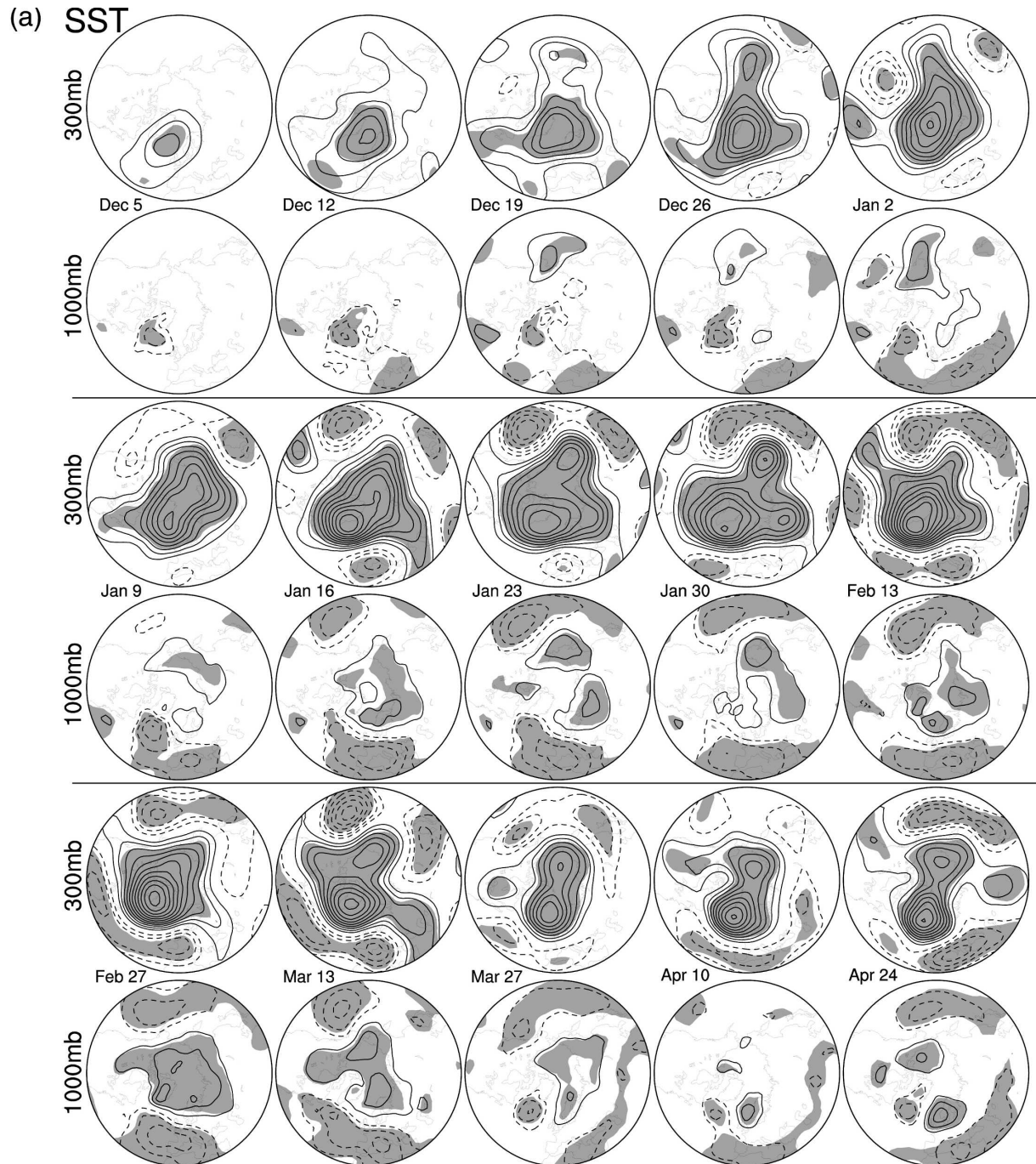


FIG. 3. As in Fig. 2, but for weekly averages over the course of the integrations (1 Dec–30 Apr). The dates correspond to the midpoint of the weekly average (e.g., 5 Dec refers to the week of 2–8 Dec). Note that, starting in February, only every other week is shown due to space limitations. (a) SST experiment; (b) ICE experiment.

which shows the spatial correlation coefficients between daily anomaly fields at 1000 and 300 hPa north of 30°N (the anomalies have been multiplied by the square root of the cosine of latitude before computing the correlation to ensure proper area weighting). A 3-day running mean was applied to the daily anomaly

fields before computing the spatial correlations to smooth the results slightly. Both the SST and ICE experiments exhibit strong negative spatial correlation coefficients within the first week, consistent with the anomaly maps shown in Fig. 3; the magnitudes of the negative correlations are larger in the SST case than the

(b) ICE

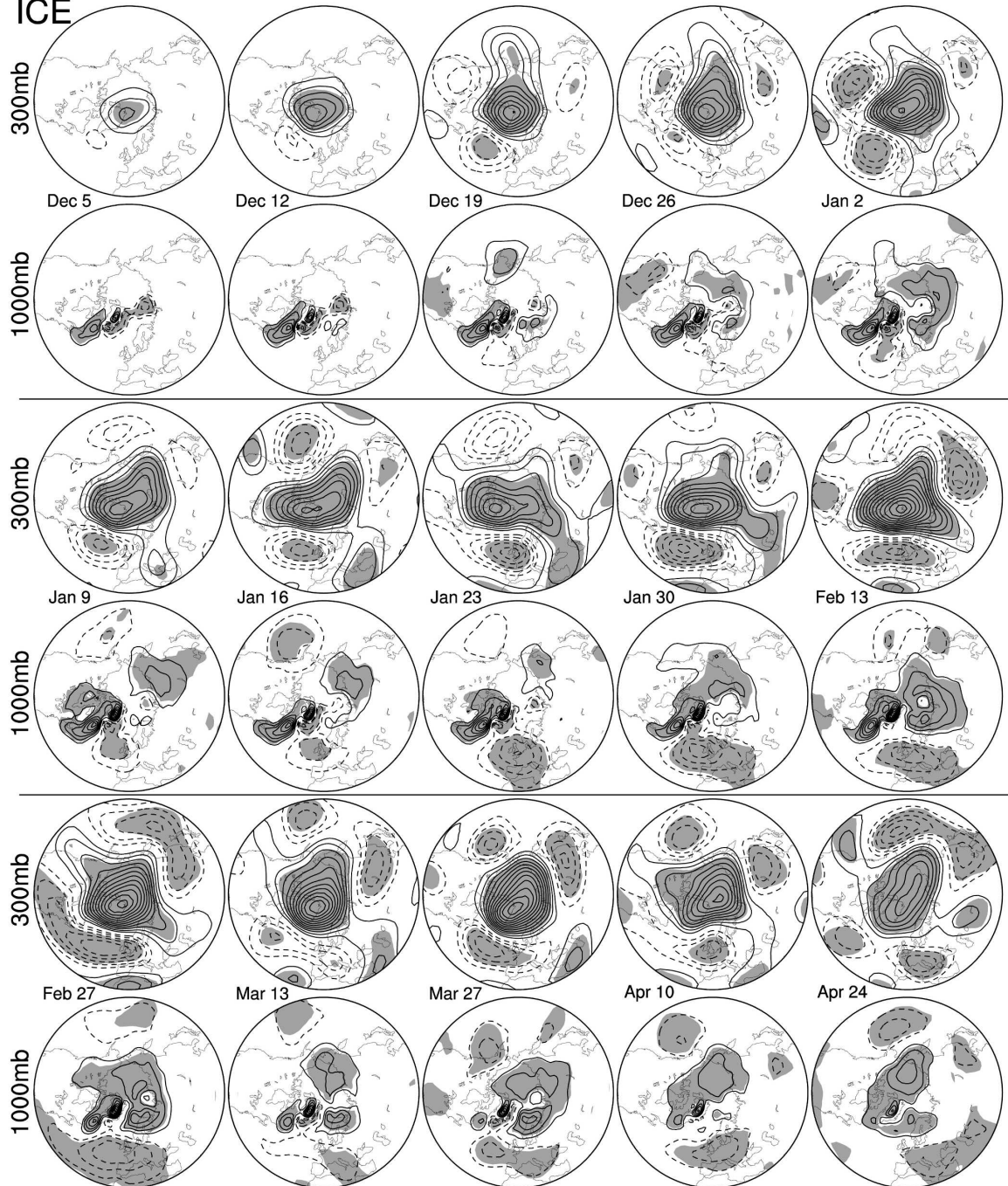


FIG. 3. (Continued)

ICE case (cf. 0.82 and 0.47) due to the larger spatial scale of the SST forcing compared to the sea ice forcing. The correlation coefficients change sign from negative to positive values (e.g., indicative of a transition from a baroclinic to an equivalent barotropic vertical structure) during the third week (the transition occurs a few days later for SST than ICE). The positive spatial cor-

relations reach similar maximum values ( $\sim 0.7$ ) from mid-January to the end of March in the SST and ICE cases; in April, the positive correlations have weakened in the SST case, but remain high in the ICE case.

The overall amplitude of the daily geopotential height responses at 1000 and 300 hPa as a function of time are summarized in Fig. 5, which shows the daily

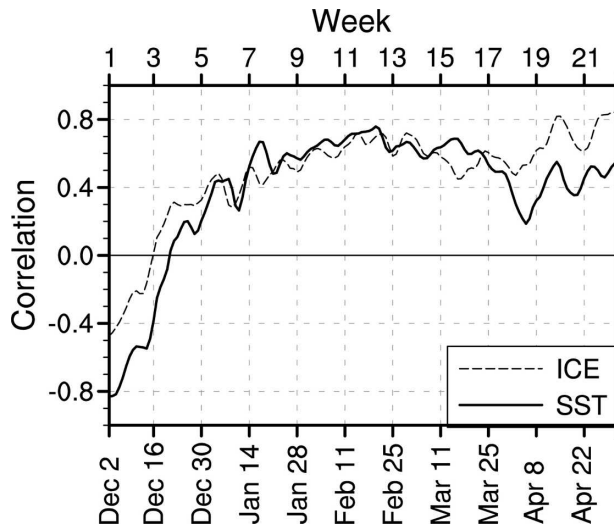


FIG. 4. Spatial correlation coefficients between daily geopotential height responses at 1000 and 300 hPa for the SST and ICE experiments. The daily data have been smoothed with a 3-day running mean filter before computing the correlations. The top and bottom horizontal axes are labeled according to week number (week 1 refers to 2–8 Dec) and calendar day, respectively.

rms values of the area-weighted anomalies averaged over the Northern Hemisphere poleward of  $30^{\circ}\text{N}$ . The rms values are approximately 3 times as large at 300 as at 1000 hPa and attain their maxima after approximately 8 weeks in the SST case and 10 weeks in the ICE case.

#### b. Role of internal variability

Following D04, we examine the relationship between the leading mode of internal variability in the control ensemble and the ensemble mean response to the imposed boundary forcing in SST and ICE. The initial (days 1–14) and time-averaged (days 15–150) geopotential height responses at 1000, 650, and 300 hPa in SST and ICE are shown in Fig. 6 (columns 1 and 2). As already noted with regard to Fig. 3, the initial responses are baroclinic and localized to the vicinity of the forcing while the time-averaged responses are equivalent barotropic and hemispheric in scale, with positive anomalies at high latitudes and negative anomalies at midlatitudes over the Atlantic and Pacific. Removing the initial response from the time-averaged response (Fig. 6, column 3) at each level yields patterns that resemble closely the leading EOF of time-averaged geopotential height anomalies in the 240-member control ensemble (Fig. 6, column 4), with spatial correlation coefficients of 0.86–0.89 for SST and 0.93–0.94 for ICE depending on level. (The leading EOF of the control ensemble is computed separately for each level using the 240 time-

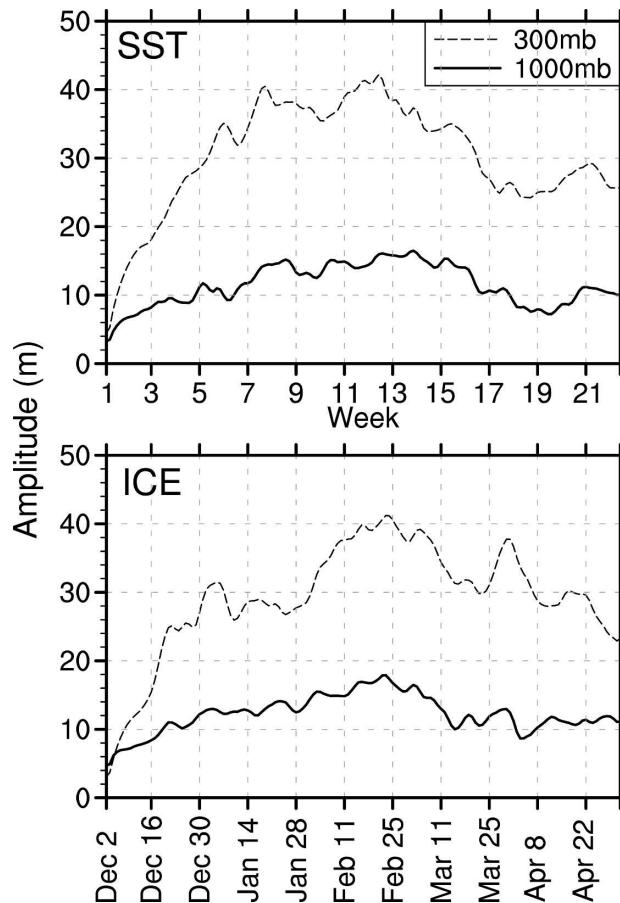


FIG. 5. Amplitudes of the daily geopotential height responses at 1000 and 300 hPa for the (top) SST and (bottom) ICE experiments. Amplitudes are defined as the area average of the rms of the height responses north of  $30^{\circ}\text{N}$ .

averaged geopotential height fields, and accounts for 32%–39% of the variance depending on level.) Note that the EOF patterns in Fig. 6 have been scaled for visual convenience by a spatial regression coefficient obtained separately for each level by projecting the pattern in column 3 (time-averaged minus initial response) onto the unscaled EOF.

Subtracting EOF1 of the control ensemble (Fig. 6, column 4) from the time-averaged response (Fig. 6, column 2) yields a residual pattern (Fig. 6, column 5) that resembles the initial response, especially in the ICE case. However, it is also apparent that the amplitude of the residual response in the mid- and upper troposphere is larger than that of the initial response. The time-averaged responses, EOF structures, and residual patterns obtained from the transient experiments (Fig. 6) are qualitatively similar to those from the equilibrium experiments shown in D04.

At what point in the transient integrations does the

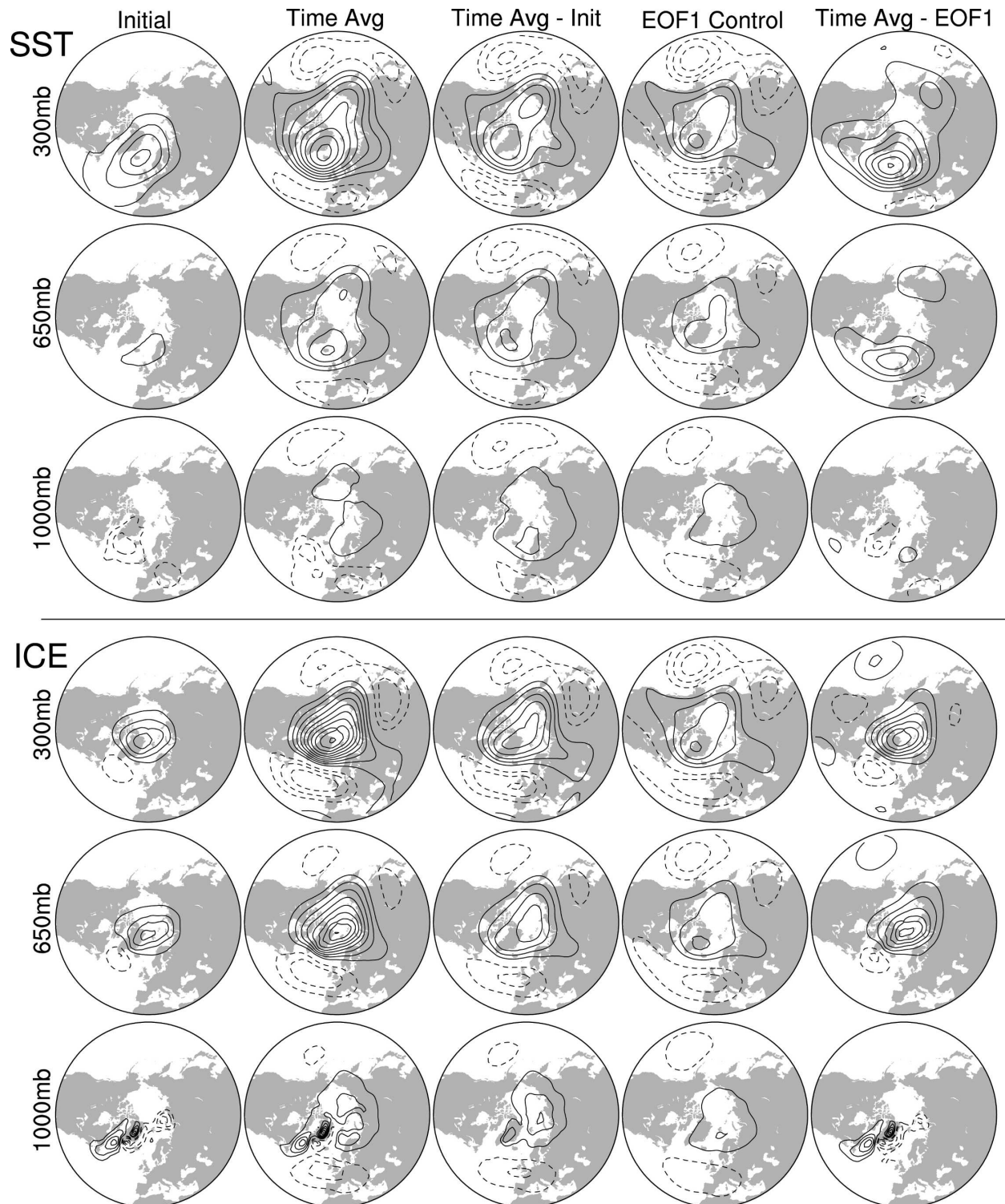


FIG. 6. Geopotential height responses at 1000, 650, and 300 hPa for the (top) SST and (bottom) ICE experiments. The contour interval in all panels is 10 m, with solid (dashed) contours denoting positive (negative) values; the zero contours have been omitted for clarity. “Initial” refers to the response averaged over the first 2 weeks (days 1–14); “Time Avg” refers to the time mean response after the second week (days 15–150); “Time Avg-Init” refers to “Time Avg” minus “Initial”; “EOF1 Control” refers to the leading EOF of the time mean of the 240 control experiments, scaled as described in the text; “Time Avg – EOF1” refers to “Time Avg” minus “EOF1 Control”.

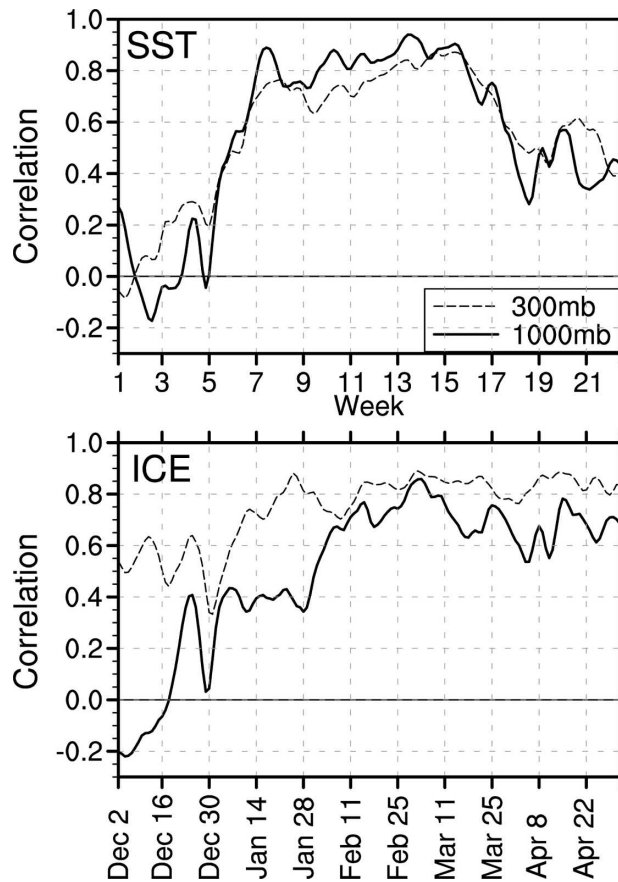


FIG. 7. Spatial correlation coefficients between the daily geopotential height responses and the leading EOF of the time-mean control ensemble at 1000 and 300 hPa, based on data north of  $30^{\circ}\text{N}$  for the (top) SST and (bottom) ICE experiments. The daily data were smoothed with a 3-point running mean before computing the spatial correlations.

response begin to resemble the leading EOF of the control ensemble? To answer this question, we have computed the daily spatial correlation coefficient between the ensemble-mean geopotential height response and the control ensemble EOF1 at 1000 and 300 hPa based on area-weighted anomalies north of  $30^{\circ}\text{N}$  (Fig. 7). Daily values of EOF1 were obtained by computing the leading EOF for each month separately and then linearly interpolating the monthly values to daily values. Using a single EOF1 pattern based on December–April averages yields very similar results (not shown). For the SST case, the response starts to resemble EOF1 around week 7 (mid-January) and continues through week 17 (late March), with spatial correlation coefficients  $\sim 0.7$ – $0.9$ . The correlation coefficients diminish in April, with values  $\sim 0.6$  at 300 hPa and  $\sim 0.4$  at 1000 hPa. For the ICE case, the correlation coefficients at the 300-hPa level increase through the course of the

integration, from values  $\sim 0.4$  in early December to  $\sim 0.85$  in late April. The higher correlation coefficients for ICE than SST in the first 6 weeks at 300 hPa reflect that the centers of action of the response in ICE are contained within those of the EOF pattern. The spatial correlation coefficients for the ICE case are considerably weaker at 1000 hPa compared to 300 hPa during the first 9 weeks due to the stronger localized response directly over the sea ice anomalies compared to the remote large-scale response.

### c. Roles of diabatic heating and transient eddies

We use the LBM of Peng et al. (2003) to diagnose the maintenance of the CCM3 response by anomalous diabatic heating and transient eddy heat and vorticity fluxes in the SST and ICE experiments. Figure 8 shows the LBM responses to diabatic heating and transient eddy fluxes in week 1, along with the corresponding CCM3 response. Note that the contour interval for the LBM responses is 5 m compared to 10 m for the GCM response. The spatial and vertical structure of the LBM response to diabatic heating is similar to the full GCM response, especially for the ICE case, although the amplitude is approximately a factor of 2 smaller in the mid- and upper troposphere. Peng et al. (2003) also found that the LBM underestimates the amplitude of the GCM by approximately a factor of 2, and attributed this shortcoming to limitations of the linear dynamics, damping prescriptions, and differences in the model configurations (note that we have not attempted to tune the dissipation parameters). The LBM response to transient eddy heat and vorticity fluxes is small compared to the response to diabatic heating at the initial stage.

The diabatic heating anomalies used to force the LBM (Fig. 9) reflect the locations of the SST and sea ice anomalies, and are largest in the lower troposphere. Note that the anomalous heating profile is shallower for sea ice than for SST, consistent with the vertical structures of the geopotential height responses shown in Fig. 8. Although the LBM captures the baroclinic structure of the GCM response, the transition between negative and positive anomalies occurs at a slightly higher altitude in the LBM than in the GCM, likely related to the different vertical resolutions of the two models.

Figure 10 shows the LBM responses to diabatic heating and transient eddy heat and vorticity fluxes for the period 15 January–1 April when the GCM response pattern is fully developed (the results are not sensitive to the precise choice of averaging period once the hemispheric character of the response has been established). The LBM response to transient eddy forcing captures much of the hemispheric, equivalent barotropic char-

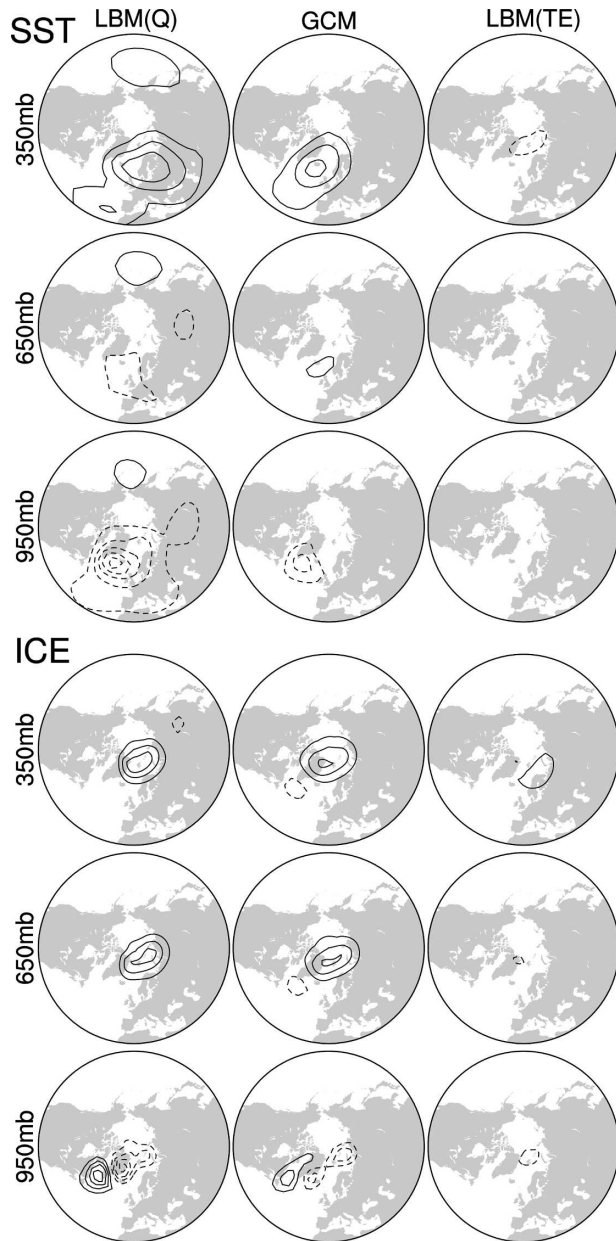


FIG. 8. LBM responses at 350, 650, and 950 hPa to diabatic heating [LBM(Q); left column] and transient eddy heat and vorticity fluxes [LBM(TE); right column] from the CCM3 SST and ICE experiments averaged over the first week. The full CCM3 responses averaged over the first week are shown in the middle column (labeled GCM). The contour interval for the LBM (CCM3) responses is 5 m (10 m), with solid (dashed) contours denoting positive (negative) values; the zero contours have been omitted for clarity. See text for details of the LBM calculations.

acter of the full GCM response in both the SST and ICE cases, although as before, the amplitude of the LBM response is approximately a factor of 2 smaller than the full GCM response. The vorticity component of the transient eddy fluxes dominates the heating com-

ponent in terms of the LBM response, although at 350 hPa, transient eddy heat fluxes substantially augment the transient eddy vorticity fluxes (Fig. 10, columns 4 and 5). These results are in keeping with previous studies regarding the relative importance of transient eddy heat and vorticity fluxes (Ting and Lau 1993).

The LBM response to diabatic heating is small compared to the response to transient eddy fluxes, and is similar in structure to that in week 1 but  $\sim 30\%$  smaller in amplitude (cf. Fig. 8). The weakening of the LBM response to diabatic heating over time reflects a reduction of the anomalous diabatic heating in the lower troposphere associated with the thermal adjustment of the atmospheric planetary boundary layer to the underlying surface temperature anomaly as shown in Fig. 9. The structure of the transient eddy vorticity flux convergence anomalies used to force the LBM (Fig. 11) corresponds approximately to that of the geopotential height response in the GCM and maximizes in the upper troposphere, consistent with previous studies (e.g., Lau and Holopainen 1984).

The temporal evolution of the contributions of diabatic heating and transient eddy heat and vorticity fluxes as diagnosed from the LBM to the full CCM3 response is summarized in Fig. 12. This diagram shows the spatial correlation and regression coefficients between the actual GCM response and the LBM responses to diabatic heating, transient eddy heat, and vorticity fluxes based upon weekly averages smoothed with a 1–2–1 binomial filter. For the SST case at 950 hPa, the contribution by diabatic heating exceeds that by transient eddy fluxes during the first 3 weeks, with spatial correlations near or exceeding 0.8. The contribution by diabatic heating gradually decays to near zero by the 10th week, while the contribution by transient eddy forcing dominates between weeks 5 and 16, with spatial correlation coefficients near 0.7 and spatial regression coefficients near 0.4. At 350 hPa, the contribution by transient eddies dominates that by diabatic heating by the third week of the simulations, with spatial correlation coefficients near 0.8 and regressions near 0.4. (In fact, the LBM response to diabatic heating at 350 hPa is negatively correlated with the GCM response between weeks 5 and 16.)

The results for the ICE case are similar to those for SST, especially at 350 hPa. However, at 950 hPa during the first two weeks of the simulations, the spatial correlation and regression coefficients between the LBM response to transient eddy fluxes and the GCM response are positive, opposite to the SST case, and the correspondence between the LBM response to diabatic heating and the GCM response is lower than that in the

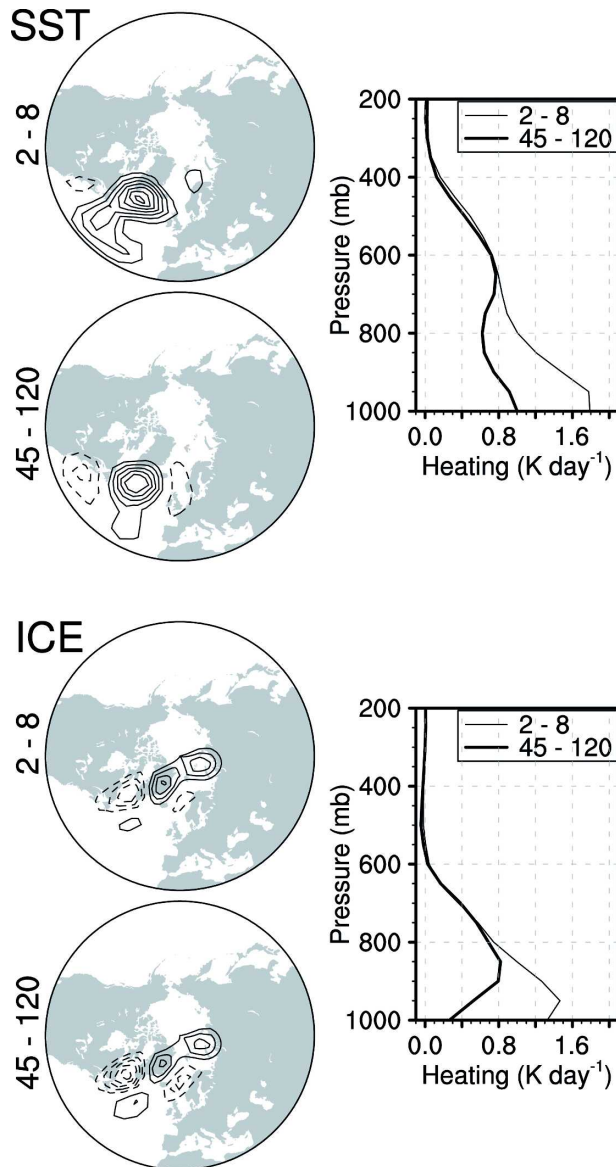


FIG. 9. (left) Vertically averaged diabatic heating responses for days 2–8 and 45–120 for the (top) SST and (bottom) ICE experiments. The contour interval is  $0.2 \text{ K day}^{-1}$  for SST and  $0.4 \text{ K day}^{-1}$  for ICE. Solid (dashed) contours denote positive (negative) values, with the zero contours omitted. (right) Vertical profiles of the diabatic heating responses for days 2–8 (thin curve) and days 45–120 (thick curve) averaged over the region of positive anomalies ( $50^{\circ}$ – $70^{\circ}\text{N}$ ,  $60^{\circ}$ – $15^{\circ}\text{W}$  for SST and  $60^{\circ}$ – $90^{\circ}\text{N}$ ,  $45^{\circ}\text{W}$ – $120^{\circ}\text{E}$  for ICE).

SST case, perhaps due to the more limited areal extent of the sea ice forcing relative to SST forcing (cf. Fig. 1).

#### 4. Summary and discussion

We have investigated the transient evolution of the winter atmospheric circulation response to prescribed

North Atlantic SST and sea ice extent anomalies using CCM3, an atmospheric general circulation model with T42 horizontal resolution and 18 levels in the vertical. Three 240-member ensemble integrations were conducted, all beginning on 1 December and ending on 30 April: a control integration in which SST and sea ice extent are set to their observed climatological seasonally varying values, an SST perturbation integration in which a seasonally varying pattern of SST anomalies is added to the mean SST field, and a sea ice perturbation integration in which a seasonally varying pattern of sea ice extent anomalies is added to the mean sea ice extent field. Different atmospheric initial conditions are used for each member of the ensembles. The SST and sea ice extent anomaly patterns are identical to those used in the equilibrium response studies of M04 and D04, and are based upon observed trends during the second half of the twentieth century. Following M04 and D04, the amplitudes of the SST (sea ice) anomalies were increased by a factor of 5 ( $\sim 2$ ) to enhance the signal-to-noise ratios of the responses, and the polarity of the SST anomalies was reversed to facilitate comparison between the atmospheric circulation responses to the two types of boundary forcing. The maintenance of the transient atmospheric response at different stages of its evolution was diagnosed by means of a linear primitive equation model forced with the diabatic heating and transient eddy heat and vorticity flux anomalies from the GCM experiments.

The initial adjustment of the atmospheric circulation to the SST or sea ice extent forcing is characterized by an out-of-phase relationship between geopotential height anomalies in the lower and upper troposphere localized to the vicinity of the forcing. This initial baroclinic response reaches maximum amplitude in  $\sim 5$ – $10$  days (not shown), and persists for 2–3 weeks. Diagnostic results from the linear primitive equation model indicate that this component of the response is forced by diabatic heating anomalies in the lower troposphere associated with surface heat flux anomalies generated by the imposed boundary forcing. This mechanism is consistent with that described by the time-independent linear model of Hoskins and Karoly (1981). The 5–10-day adjustment time for the initial baroclinic response agrees well with that found in the single-column model experiments of Chase et al. (2002) and Tsukernik et al. (2004) in which a polar atmospheric column is subjected to open water heating or surface cooling.

Following the initial baroclinic stage of adjustment, the response becomes progressively more barotropic and increases in both spatial extent and magnitude. The equilibrium stage of adjustment is reached in 2–2.5 months, and is characterized by an equivalent barotro-

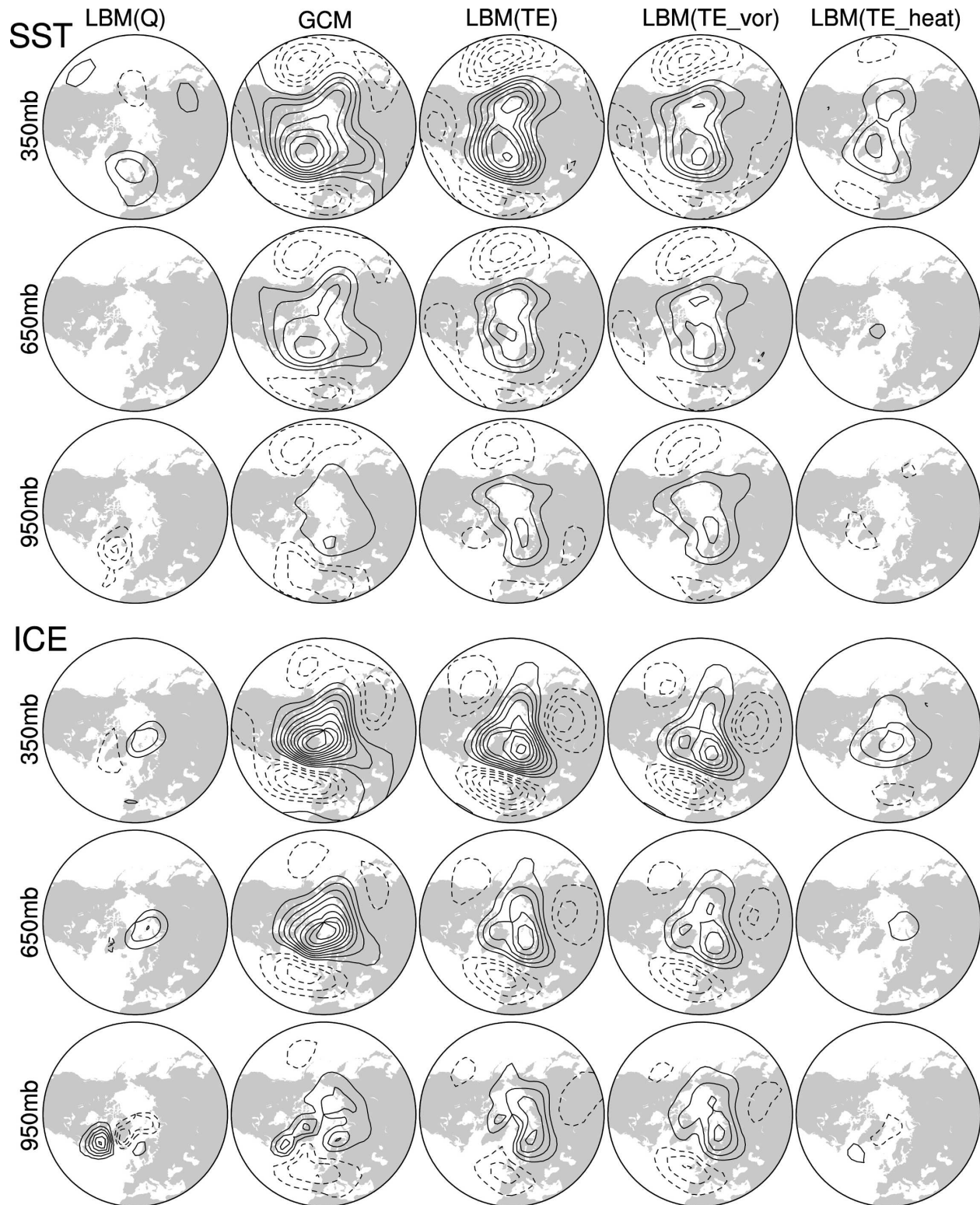


FIG. 10. As in Fig. 8, but for the average of days 45–120. The 4th and 5th columns show the LBM responses to transient eddy flux convergences of vorticity [LBM(TE\_vor)] and heat [LBM(TE\_heat)].

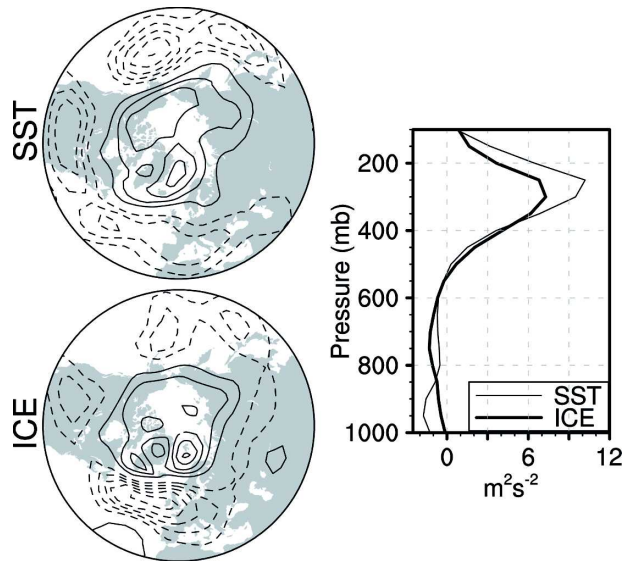


FIG. 11. (left) Vertically averaged transient eddy vorticity flux convergence response averaged over days 45–120 for the (top) SST and (bottom) ICE experiments. The contour interval is  $0.8 \text{ m}^2 \text{ s}^{-2}$ . Solid (dashed) contours denote positive (negative) values, with the zero contours omitted. (right) Vertical profiles of the transient eddy vorticity flux convergence responses for days 45–120 averaged north of  $55^\circ\text{N}$  from the SST experiment (thin curve) and ICE experiment (thick curve).

pic structure that resembles the hemispheric NAO–NAM pattern, the model’s leading internal mode of circulation variability over the Northern Hemisphere. The maximum amplitude of the equilibrium response is approximately 2–3 times larger than that of the initial response. The equilibrium response is maintained primarily by nonlinear transient eddy fluxes of vorticity (and, to a lesser extent, heat), with diabatic heating making a limited contribution in the vicinity of the forcing. The maintenance of the equilibrium geopotential height response by transient eddy vorticity fluxes is consistent with numerous earlier studies (e.g., Kushnir and Lau 1992; Ting and Peng 1995; Peng and Whitaker 1999; Peng et al. 2003).

The evolution of the transient response follows the mechanistic scenario put forth by Peng and Whitaker (1999), and is qualitatively similar to the transient adjustment process obtained in a three-level quasigeostrophic model by Ferreira and Frankignoul (2005). The 2–2.5-month time scale for the establishment of the equilibrium NAO–NAM response in this study is shorter than the 3–4 months obtained by Ferreira and Frankignoul (2005), although we note that both are considerably longer than the  $\sim 10$  days that are generally assumed. A number of factors may contribute to the different adjustment times for the NAO–NAM in

our study and that of Ferreira and Frankignoul, including: different types of atmospheric models (18-level GCM at T42 resolution versus three-layer quasigeostrophic model at T31 resolution); different North Atlantic SST forcing patterns; and different treatments of the seasonal cycle (seasonally varying conditions versus perpetual December–February conditions).

We cannot directly address the issue of how seasonal changes in the background state, in particular the location and strength of the storm tracks, may impact the adjustment time, amplitude, and pattern of the equilibrium response in CCM3 without additional experiments in which the background state is kept fixed. However, we note that the North Atlantic and Pacific storm tracks are already well established by the first week of December, the starting date for our experiments (not shown). Had our experiments begun a month earlier, we speculate that the adjustment time for the NAO–NAM response might have been longer considering that the transient eddy–mean flow interactions are likely to be weaker in November than December. On the other hand, the reduction of the NAO–NAM response in April compared to February and March is likely to be in part a consequence of the seasonal weakening of the storm track, especially in the sea ice experiment where the forcing does not change appreciably over the course of the integrations (cf. Fig. 1).

One of the motivations for the current study was to investigate the physical basis for D04’s empirical decomposition of the equilibrium response into a component that projects onto the model’s leading mode of intrinsic variability (termed the “indirect response”) and a component that is the residual from that projection (termed the “direct response”). Based upon the different spatial and vertical structures of these components, D04 speculated that transient eddy forcing maintains the indirect response while diabatic heating maintains the direct response. Performing the same empirical decomposition on the time-averaged transient response, we found similar patterns for the direct and indirect responses as D04. We further noted that the direct response resembles the initial transient response. Thus, the direct and indirect responses are largely consistent with D04’s physical interpretation by virtue of their similarity to the initial and equilibrium responses, respectively. However, transient eddy forcing may also contribute to the direct response, especially in the mid- and upper troposphere where the direct response is larger than the initial response. Thus, the empirical decomposition technique of D04, while physically insightful, may not fully isolate the diabatically forced and transient eddy-forced components of the response.

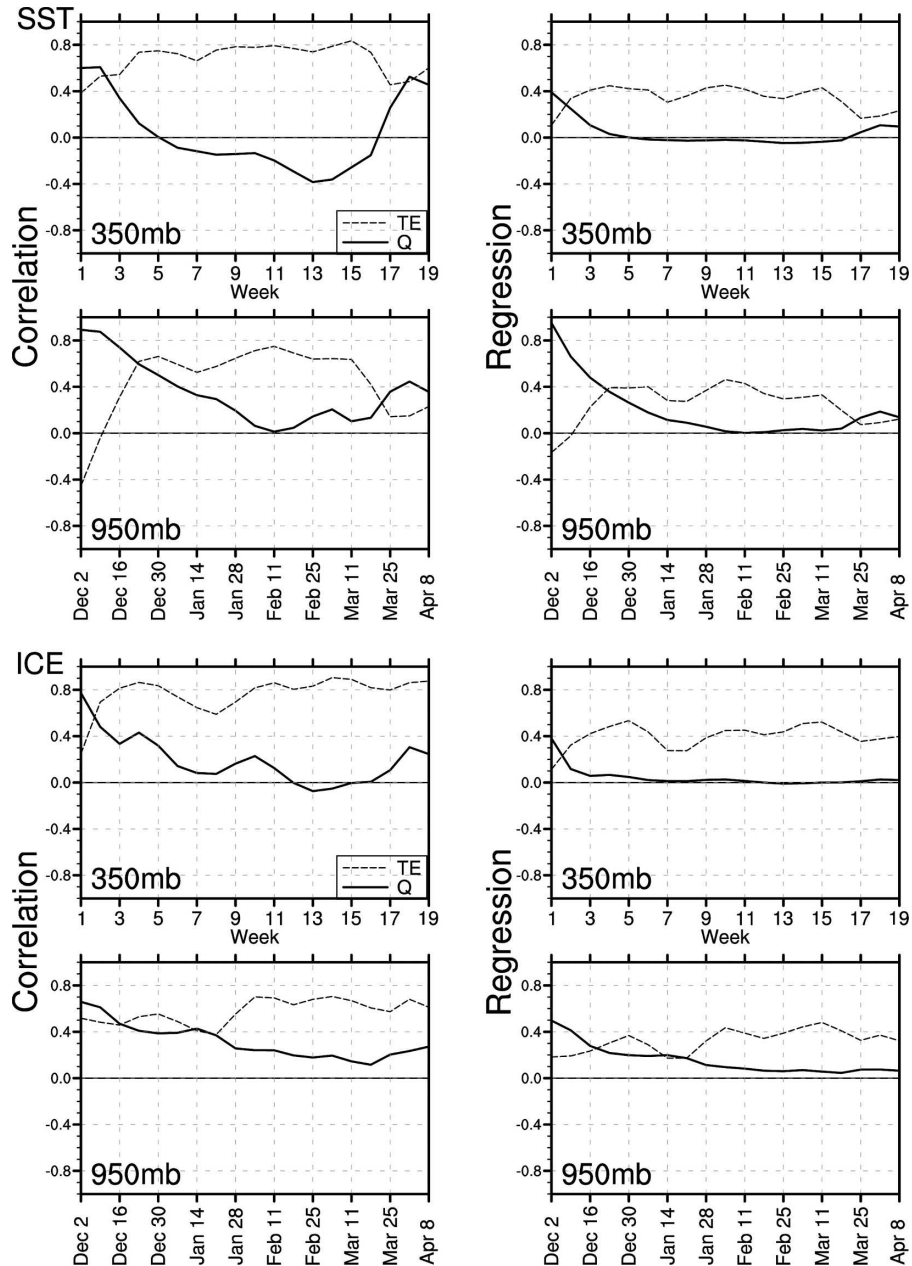


FIG. 12. (left) Spatial correlation and (right) regression coefficients between the full CCM3 and the LBM responses to diabatic heating ( $Q$ ) and transient eddy heat and vorticity fluxes (TE) based upon weekly averages smoothed with a 1–2–1 binomial filter for the (top) SST and (bottom) ICE experiments. Spatial correlation/regression coefficients are based upon geopotential height responses at 350 hPa and 950 hPa. See text for details.

As discussed in M04 and D04, the atmospheric circulation response to the imposed sea ice anomaly trend constitutes a moderate (40%) negative feedback: it is opposite in sign to, and approximately 40% of the magnitude of, the atmospheric circulation anomaly pattern that originally forced the sea ice anomaly trend. The

sign of this feedback is maintained in an additional integration of the model in which both the observed SST and sea ice anomaly trends are jointly imposed, even though the atmospheric response to the observed SST trend represents a positive (but weak) feedback (see M04 and D04). Since the amplitude of the atmospheric

response was found to scale approximately linearly with the amplitude of the SST or sea ice forcing for a given forcing polarity (M04 and D04), the magnitude of this feedback is likely to be similar for more realistic forcing amplitudes than those used here.

The 2–2.5-month adjustment time scale of the NAO–NAM to imposed patterns of North Atlantic SST and sea ice anomalies found in this study is comparable to the persistence time scale of the SST and sea ice anomalies themselves (Frankignoul and Hasselmann 1977; Deser et al. 2003). Thus, the extratropical atmosphere and ocean mixed layer (or sea ice) should be viewed as continually and mutually adjusting systems over this time scale. A recent modeling study by Cassou et al. (2007) examining the mutual transient adjustment of the atmosphere and ocean mixed layer to a subsurface ocean temperature anomaly in the extratropical North Atlantic supports this view.

The results obtained in this study pertain to one model (CCM3) forced with one particular pattern of North Atlantic SST (or sea ice) anomalies. It is likely that the time scale for the establishment of the equilibrium atmospheric response, as well as its amplitude, pattern, and duration may vary considerably with the model and forcing characteristics. Additional experiments with different forcing patterns and different atmospheric models, as well as coupled ocean–atmosphere models, are needed to further our understanding of the equilibrium atmospheric response to extratropical SST and sea ice anomalies.

*Acknowledgments.* Support from NOAA's CLIVAR Program to C. Deser is gratefully acknowledged. We thank the three reviewers for their constructive and thoughtful comments that helped to improve the manuscript.

#### REFERENCES

- Branstator, G., 1992: The maintenance of low frequency atmospheric anomalies. *J. Atmos. Sci.*, **49**, 1924–1945.
- Cassou, C., C. Deser, and M. A. Alexander, 2007: Investigating the impact of reemerging sea surface temperature anomalies on the winter atmospheric circulation over the North Atlantic. *J. Climate*, **20**, 3510–3526.
- Chase, T. N., B. Herman, R. A. Pielke Sr., X. Zeng, and M. Leuthold, 2002: A proposed mechanism for the regulation of minimum mid-tropospheric temperatures in the Arctic. *J. Geophys. Res.*, **107**, 4193, doi:10.1029/2001JD001425.
- Deser, C., J. E. Walsh, and M. S. Timlin, 2000: Arctic sea ice variability in the context of recent atmospheric circulation trends. *J. Climate*, **13**, 617–633.
- , M. A. Alexander, and M. S. Timlin, 2003: Understanding the persistence of sea surface temperature anomalies in mid-latitudes. *J. Climate*, **16**, 57–72.
- , G. Magnusdottir, R. Saravanan, and A. S. Phillips, 2004: The effects of North Atlantic SST and sea-ice anomalies on the winter circulation in CCM3. Part II: Direct and indirect components of the response. *J. Climate*, **17**, 877–889.
- Ferreira, D., and C. Frankignoul, 2005: The transient atmospheric response to midlatitude SST anomalies. *J. Climate*, **18**, 1049–1067.
- Frankignoul, C., and K. Hasselmann, 1977: Stochastic climate models. Part 2: Application to sea-surface temperature variability and thermocline variability. *Tellus*, **29**, 289–305.
- Hack, J. J., J. T. Kiehl, and J. W. Hurrell, 1998: The hydrologic and thermodynamic characteristics of the NCAR CCM3. *J. Climate*, **11**, 1179–1206.
- Hall, N. M. J., J. Derome, and H. Lin, 2001: The extratropical signal generated by a midlatitude SST anomaly. Part I: Sensitivity at equilibrium. *J. Climate*, **14**, 2035–2053.
- Hendon, J. J., and D. L. Hartmann, 1982: Stationary waves on a sphere: Sensitivity to thermal feedback. *J. Atmos. Sci.*, **39**, 1906–1920.
- Hoskins, B. J., and D. Karoly, 1981: The steady linear response of a spherical atmosphere to thermal and orographic forcing. *J. Atmos. Sci.*, **38**, 1179–1196.
- Hurrell, J. W., 1995: Decadal trends in the North Atlantic Oscillation: Regional temperatures and precipitation. *Science*, **269**, 676–679.
- , J. J. Hack, B. A. Boville, D. L. Williamson, and J. T. Kiehl, 1998: The dynamical simulation of the NCAR Community Climate Model version 3 (CCM3). *J. Climate*, **11**, 1207–1236.
- Kiehl, J. T., J. J. Hack, G. B. Bonan, B. A. Boville, D. L. Williamson, and P. J. Rasch, 1998: The National Center for Atmospheric Research community climate model: CCM3. *J. Climate*, **11**, 1131–1149.
- Kushnir, Y., and N.-C. Lau, 1992: The general circulation model response to a North Pacific SST anomaly: Dependence on time scale and pattern polarity. *J. Climate*, **5**, 271–283.
- , W. A. Robinson, I. Blade, N. M. J. Hall, S. Peng, and R. Sutton, 2002: Atmospheric GCM response to extratropical SST anomalies: Synthesis and evaluation. *J. Climate*, **15**, 2233–2256.
- Lau, N.-C., and E. O. Holopainen, 1984: Transient eddy forcing of the time-mean flow as identified by geopotential tendencies. *J. Atmos. Sci.*, **41**, 313–328.
- Li, Z. X., 1999: Ensemble atmospheric GCM simulation of climate interannual variability from 1979 to 1994. *J. Climate*, **12**, 986–1001.
- , and S. Conil, 2003: Transient response of an atmospheric GCM to North Atlantic SST anomalies. *J. Climate*, **16**, 3993–3998.
- Magnusdottir, G., C. Deser, and R. Saravanan, 2004: The effects of North Atlantic SST and sea-ice anomalies on the winter circulation in CCM3. Part I: Main features and storm-track characteristics of the response. *J. Climate*, **17**, 857–876.
- Peng, S., and J. S. Whitaker, 1999: Mechanisms determining the atmospheric response to midlatitude SST anomalies. *J. Climate*, **12**, 1393–1408.
- , and W. A. Robinson, 2001: Relationships between atmospheric internal variability and the responses to an extratropical SST anomaly. *J. Climate*, **14**, 2943–2959.
- , —, and S. Li, 2003: Mechanisms for the NAO responses to the North Atlantic SST tripole. *J. Climate*, **16**, 1987–2004.
- Raynor, N. A., E. B. Horton, D. E. Parker, C. K. Folland, and

- R. B. Hackett, 1996: Version 2.3 of the global sea ice and sea surface temperature data set 1903–1994. Hadley Centre Tech. Note CRTN 74, 21 pp. [Available from Hadley Centre for Climate Prediction and Research, London Rd., Bracknell, Berkshire RG12 2SY, United Kingdom.]
- Robinson, W. A., 2000: Review of WETS—The workshop on extratropical SST anomalies. *Bull. Amer. Meteor. Soc.*, **81**, 567–577.
- Thompson, D. W. J., and J. M. Wallace, 1998: The Arctic Oscillation signature in the wintertime geopotential height and temperature fields. *Geophys. Res. Lett.*, **25**, 1297–1300.
- Ting, M., and N.-C. Lau, 1993: A diagnostic and modeling study of the monthly mean wintertime anomalies appearing in a 100-year GCM experiment. *J. Atmos. Sci.*, **50**, 2845–2867.
- , and S. Peng, 1995: Dynamics of the early and middle winter atmospheric responses to northwest Atlantic SST anomalies. *J. Climate*, **8**, 2239–2254.
- Tsukernik, M., T. N. Chase, M. C. Serreze, R. G. Barry, R. Pielke Sr., B. Herman, and X. Zeng, 2004: On the regulation of minimum mid-tropospheric temperatures in the Arctic. *Geophys. Res. Lett.*, **31**, L06112, doi:10.1029/2003GL018831.
- Walter, K., U. Luksch, and K. Fraedrich, 2001: A response climatology of idealized midlatitude thermal forcing experiments with and without a storm track. *J. Climate*, **14**, 467–484.